Energy conversion at the Earth's magnetopause using single and multispacecraft methods

C. R. Anekallu,[1,2] M. Palmroth,[1] T. I. Pulkkinen,[3] S. E. Haaland,[4,5] E. Lucek,[6] and I. Dandouras[7,8]

Received 26 April 2011; revised 26 August 2011; accepted 28 August 2011; published 5 November 2011.

[1] We present a small statistical data set, where we investigate energy conversion at the magnetopause using Cluster measurements of magnetopause crossings. The Cluster observations of magnetic field, plasma velocity, current density and magnetopause orientation are needed to infer the energy conversion at the magnetopause. These parameters can be inferred either from accurate multispacecraft methods, or by using single-spacecraft methods. Our final aim is a large statistical study, for which only single-spacecraft methods can be applied. The Cluster mission provides an opportunity to examine and validate single-spacecraft methods against the multispacecraft methods. For single-spacecraft methods, we use the Generic Residue Analysis (GRA) and a standard one-dimensional current density method using magnetic field measurements. For multispacecraft methods, we use triangulation (Constant Velocity Approach - CVA) and the curlometer technique. We find that in some cases the single-spacecraft methods yield a different sign for the energy conversion than compared to the multispacecraft methods. These sign ambiguities arise from the orientation of the magnetopause, choosing the interval to be analyzed, large normal current and time offset of the current density inferred from the two methods. By using the Finnish Meteorological Institute global MHD simulation GUMICS-4, we are able to determine which sign is likely to be correct, introducing an opportunity to correct the ambiguous energy conversion values. After correcting the few ambiguous cases, we find that the energy conversion estimated from single-spacecraft methods is generally lower by 70% compared to the multispacecraft methods.

Citation: Anekallu, C. R., M. Palmroth, T. I. Pulkkinen, S. E. Haaland, E. Lucek, and I. Dandouras (2011), Energy conversion at the Earth's magnetopause using single and multispacecraft methods, *J. Geophys. Res.*, *116*, A11204, doi:10.1029/2011JA016783.

1. Introduction

[2] The energy input to the magnetosphere is primarily controlled by the solar wind and the interplanetary magnetic field (IMF). The energy transfer and conversion occurs mainly by reconnection between the IMF and the terrestrial field lines [e.g., *Dungey*, 1961], while also viscous interactions at the magnetopause surface transfer energy [*Axford and Hines*, 1961]. The question of how much energy is converted at the magnetopause and how it is distributed within the magnetosphere and ionosphere is one of the most important questions in space physics. Due to a limited satellite coverage of the magnetosphere this question is difficult to answer observationally on global scales. However, empirical estimates like the ϵ parameter [*Akasofu*, 1981] are widely used as proxies for the global energy input. According to the current theoretical understanding [e.g., *Lundin and Evans*, 1985], magnetic energy is converted into a kinetic form in the dayside load region during low-latitude reconnection, while in the tail the energy is converted from the kinetic into magnetic form in a generator. In the tail lobe generator, the energy conversion occurs at the expense of solar wind kinetic energy sweeping the open field lines tailward.

[3] *Palmroth et al.* [2003, 2006] used the three-dimensional MHD simulation, Grand Unified Magnetosphere Ionosphere Coupling Simulation (GUMICS), to investigate the total energy transfer at the magnetopause as a function of IMF and the dynamic pressure. They found that the ϵ parameter largely agrees with the simulation energy transfer, but there are also differences in the time history as well as due to solar wind density, which is not represented in ϵ. *Laitinen et al.* [2006] developed a method to estimate the local energy conversion

[1]Finnish Meteorological Institute, Helsinki, Finland.
[2]Department of Physics, University of Helsinki, Helsinki, Finland.
[3]School of Electrical Engineering, Aalto University, Aalto, Finland.
[4]Max-Planck-Institute for Solar System Research, Katlenburg-Lindau, Germany.
[5]Also at Department of Physics and Technology, University of Bergen, Bergen, Norway.
[6]Space and Atmospheric Physics, Imperial College, London, UK.
[7]CESR, Université de Toulouse, Toulouse, France.
[8]Also at CNRS, Toulouse, France.

0148-0227/11/2011JA016783

through the magnetopause in the GUMICS simulation, again as a function of IMF and dynamic pressure. Their method essentially computes the divergence of the Poynting flux integrated across the magnetopause. *Laitinen et al.* [2006, 2007] found that the GUMICS simulation is in good accordance with the theoretical understanding of the load and generator regions, as the magnetic energy was destroyed in the dayside reconnection region, while at the tail lobes the energy is converted from the kinetic to magnetic form. They also estimated the total amount of converted energy as well as compared the results to those obtained earlier in the energy transfer estimations [*Palmroth et al.*, 2006].

[4] While the energy conversion is difficult to address globally using observations, local methods using *in situ* observations exist. Cluster mission provides an opportunity to estimate local energy conversion taking the advantage of the multispacecraft techniques. Recently, *Rosenqvist et al.* [2006] used Cluster data to calculate energy conversion at the magnetopause with

$$\mathbf{Q} = \int \{(\mathbf{J} \times \mathbf{B}) \cdot \mathbf{V}\} \, |V_{mp}| dt \; \left(Wm^{-2}\right) \tag{1}$$

where $\mathbf{J}$ is current density, $\mathbf{B}$ is magnetic field, $\mathbf{V}$ is the plasma velocity and V_{mp} is the magnetopause velocity in the normal direction. In a time-independent case, it is straightforward to show that $\mathbf{J} \times \mathbf{B} \cdot \mathbf{V}$ equals $\mathbf{E} \cdot \mathbf{J}$, which then equals to the (negative of) the Poynting vector divergence that can be used to estimate local energy conversion [*Palmroth et al.*, 2011]. Notice that $|V_{mp}|dt = dl$, represents integration over the width of the magnetopause. The magnetopause velocity V_{mp} can be positive or negative but in the energy conversion computation only the absolute value matters. This is because physically the sign of the energy conversion should be determined by $\mathbf{J} \times \mathbf{B} \cdot \mathbf{V}$ and not the magnetopause velocity, which is only used to convert the spatial integration measure into temporal form and hence only concerns the size of the subintegrations in the final outcome. *Rosenqvist et al.* [2006] found that the energy conversion can be milliwatts locally during a major magnetic storm, and using this value they also obtained a crude estimate for the total energy transfer by making assumptions on the energy transfer spatial distribution at the magnetopause.

[5] *Rosenqvist et al.* [2008b] used Cluster observations and compared the local energy conversion rate at the magnetopause with the results of the BATSRUS MHD simulation. They found that the Cluster estimate of the energy conversion was in good accordance with the simulation results after they artificially lowered the spacecraft trajectory in the simulation toward the subsolar position. *Palmroth et al.* [2011] argued that this discrepancy with the simulation results at the original spacecraft trajectory is possibly produced by a selection of a locally disturbed current system that does not represent the global Chapman-Ferraro pattern, while at another time at the same day the crossing of the global Chapman-Ferraro current system yields a good accordance with the GUMICS simulation without changing the spacecraft position in the simulation.

[6] The vast amount of data from more than 10 years of Cluster operation gives the opportunity to verify the simulation results of global energy conversion. However, the accurate multispacecraft methods depend on the inter-spacecraft distance, as for instance the curlometer technique [*Robert et al.*, 1998; *Dunlop et al.*, 2002] gives the best estimate of the current density when the spacecraft separation is small. This in turn reduces the number of crossings that can be used to accurately verify the simulation results, because the spacecraft separation is suitably small only during Feb - Jun, 2002 and from July 2003 till Apr 2004. Hence, a large statistical study requires utilization of single-spacecraft methods, which need to be validated first against multispacecraft methods.

[7] In this study we prepare for the future large statistical study and validate the single-spacecraft methods against multispacecraft methods in light of the energy conversion methodology first presented by *Rosenqvist et al.* [2006]. The paper is organized as follows: Section 2 describes the data and methods used, while Section 3 presents the results on the orientation and speed of the magnetopause from both single and multispacecraft methods. In section 4, we present energy conversion estimates from a few cases, and in particular we illustrate the caveats associated in estimating the energy conversion from spacecraft measurements. In section 5, we present results of energy conversion in a subset data base [*Panov et al.*, 2008], for which the spacecraft separation is suitable for validating the single-spacecraft methods. Section 6 presents discussion of the results and section 7 ends the paper with a summary of the results.

2. Data and Methods

[8] We use data from the Cluster Ion Spectrometry (CIS) [*Réme et al.*, 2001] experiment, Fluxgate Magnetometer (FGM) [*Balogh et al.*, 2001] onboard the ClusterII spacecraft [*Escoubet et al.*, 2001]. The CIS experiment produces the full three dimensional ion distributions with temporal resolution of 4 s, at the spin rate of the satellite. CIS comprises of two instruments, Hot Ion Analyzer (HIA) and time-of-flight Composition Distribution Function (CODIF) analyzer. Here we analyze plasma velocity, density and temperature from HIA and also CODIF, when there are data gaps in HIA recordings. From FGM, we use 5 Hz resolution magnetic field data to obtain accurate timing information for multispacecraft analysis techniques, while otherwise we use 0.25 Hz data to compute the energy conversion estimates.

[9] Using classical conservation laws and measurements from a single-spacecraft, *Sonnerup et al.* [2006] presented an analytical solution to the minimum-residue problem to find general formulae for the speed and the orientation of a plasma discontinuity. This approach, Generic Residue Analysis (GRA), generalizes earlier single-spacecraft methods, such as the minimum Faraday residue, MFR [*Khrabrov and Sonnerup*, 1998a] and the minimum mass flux residue, MMR [*Sonnerup et al.*, 2004] and yields a velocity vector for magnetopause motion and a covariance matrix. The covariance matrix is used to obtain three eigenvalues and their eigenvectors, which form the coordinate axes moving with the discontinuity. The eigenvector corresponding to the minimum eigenvalue represents the normal of the discontinuity. In the generalized approach *Sonnerup et al.* [2006] used MHD conservation laws for mass (MMR), linear momentum (minimum linear momentum residue, MLMR), total energy (minimum total energy residue, MTER), entropy (minimum entropy residue, MER) and other conservation laws, such as the absence of magnetic monopoles (minimum variance analysis on magnetic field, MVAB) and conservation of magnetic flux (MFR). In

case of MVAB, magnetopause velocity is velocity in the deHoffmann-Teller frame [*de Hoffmann and Teller*, 1950]. A combination of all these methods (COM) is obtained by a weighting procedure, where a large ratio between the intermediate and the minimum eigenvalues gives a large weight for a particular method. Some of the conservation laws mentioned above use only magnetic field data, some use only plasma data, and some use both the magnetic field and plasma data. Hence, the idea behind GRA is to make use of all the data available from a single spacecraft and to combine different conservation laws to obtain a composite (COM) prediction for orientation and motion of the magnetopause.

[10] *Sonnerup et al.* [2006] tested the GRA methods using a benchmark magnetopause crossing. They applied the MVAB method on the magnetic field data from all four Cluster spacecraft, and chose the average of the four normals as the reference normal. They reported that all of the above residue methods yielded normals that are within 9 degrees of the reference normal, while the COM method is within 3 degrees from the reference. The magnetopause velocities from all the methods agree in sign, and the magnitudes are within the standard uncertainty estimates given by *Sonnerup and Scheible* [1998]. GRA can also be constrained with *a priori* knowledge of the type of discontinuity, For example, in case of a tangential discontinuity the net magnetic field across the discontinuity is assumed zero. In this paper we employ GRA by using four conservation laws, namely MVAB, MFR, MMR and MER and deduce a combined frame using the weighting function used by *Sonnerup et al.* [2006]. We use both magnetic field data and plasma data from Cluster-1 spacecraft and the composite method (COM) is a combination of the four methods mentioned. We performed the analysis on a single nest with a window size (i.e., number of data points) that varies from crossing to crossing. For each crossing sufficient care was taken so that the window size includes the full magnetopause crossing as well as data from either side of the magnetopause.

[11] Multispacecraft missions provide a special opportunity to determine the orientation and the speed of plasma discontinuities using the positions and the times at which different spacecraft encounter the discontinuity. *Russell et al.* [1983] presented the first method based on timing and applied it to interplanetary shocks. This method, called the constant velocity approach (CVA) assumes that the discontinuity is moving with constant velocity and requires the spacecraft positions and crossing times from all four spacecraft. Recently, *Haaland et al.* [2004] developed a similar method called the constant thickness approach (CTA), where the discontinuity is assumed to have a constant thickness. In addition to the spacecraft positions and crossing times, CTA requires the durations of the discontinuity. Noting that neither CVA nor CTA will generally be strictly true, *Paschmann et al.* [2005] derived a combination of CVA and CTA, where the magnetopause thickness variation is minimized. This method, sometimes referred to as MTV (for Minimized Thickness Variation) yields a single orientation of the magnetopause, but with different thicknesses and velocities for each individual spacecraft. For both CVA and CTA methods, accurate timing is essential in order to estimate orientation and speed of the discontinuity reliably. The timing can be obtained from any measured quantity showing a well-defined profile during the crossing. In this paper, we obtain the timing information from FGM data, which are first converted into boundary normal frame using MVAB, because the magnetopause crossing is best visible in the magnetic field component along the maximum variance direction. The crossing times are obtained by performing a cross-correlation analysis, where the maximum variance component from the satellite that first sees the magnetopause is used as a reference. In this study we use CVA to obtain the normal (N-direction) and speed of the magnetopause from multiple spacecraft. The projection of Earth's dipole on to the plane perpendicular to the normal forms the L-direction and the M-direction completes the right handed orthogonal system L-M-N [*Russell and Elphic*, 1978, 1979].

[12] The current density has traditionally been estimated from magnetic field measurements of a single-spacecraft making use of Ampére's law. The single-spacecraft methods assume that the current layer is planar and one-dimensional, and that no current flows along the layer normal. The spatial gradients needed in Ampére's law are derived from the temporal gradients of the magnetic field, making use of the normal component of the spacecraft velocity relative to the current layer (V_N). With these assumptions, the current density in boundary normal coordinates is given by

$$\begin{pmatrix} j_L(t) \\ j_M(t) \\ j_N(t) \end{pmatrix} = \frac{1}{\mu_0 V_N} \begin{pmatrix} -\dfrac{\triangle B_M(t)}{\triangle t} \\ \dfrac{\triangle B_L(t)}{\triangle t} \\ 0 \end{pmatrix}, \tag{2}$$

where μ_0 is the permeability of free space. In this paper we use equation (2) to obtain the magnetopause current density using single-spacecraft measurements.

[13] *Robert et al.* [1998] presented a method to infer current density using magnetic field measurements of multiple spacecraft. This method, named as curlometer, evaluates Ampére's law by constructing the curl of the magnetic field from the position vectors and the magnetic field observations from at least four spacecraft. Curlometer is reliable when the spacecraft separation is smaller than the size of the current layer. *Dunlop et al.* [2002] applied the curlometer technique to estimate the magnetopause current density from the Cluster four point measurements. They assessed the quality of the current based on the ratio between the divergence and the magnitude of the curl of the magnetic field; if this ratio is below 0.5 (~50%), the current density from the curlometer is reliable. In this paper, we use also the curlometer technique to obtain the magnetopause current density.

[14] In this study we use a subset of magnetopause crossings database presented by *Panov et al.* [2008]. These crossings are chosen when the interspacecraft distance between Cluster spacecraft is small such that magnetopause current density can reliably be estimated from curlometer while the normal and velocity of the magnetopause are estimated using the constant velocity approach (CVA). Figure 1 presents an overview of Cluster-1 locations during the subset of crossings. Figure 1a shows the distribution of the events in x-direction, and Figure 1b shows the position of the spacecraft in y-z plane. Among the events used in this study, almost all crossings are in the northern hemisphere (inbound crossings), and most of the crossings are on the dayside.

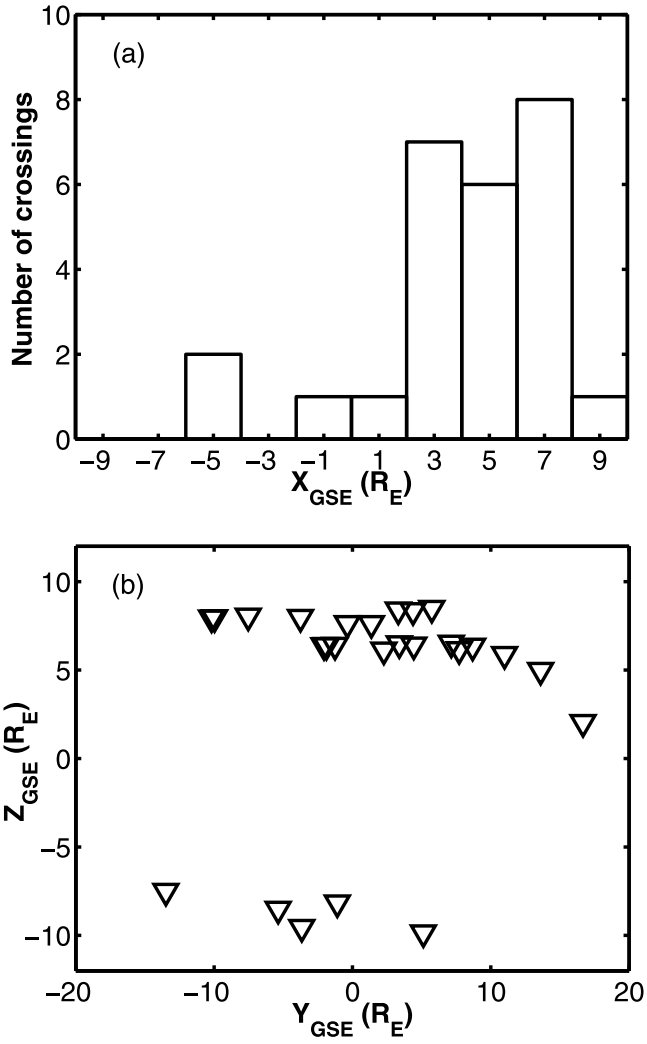

Figure 1. Overview of the locations of Cluster spacecraft, in GSE coordinates, during the magnetopause crossings used in this study. (a) The distribution of the crossings in x direction; (b) the position of the spacecraft in y-z plane.

[15] Figure 2 illustrates the types of magnetopause crossings evaluated in this study. Cluster spacecraft 1 was on an outbound crossing on 14 December, 2003, during which it was traversing the dayside magnetopause in the northern hemisphere. Shown in Figures 2a–2e are omnidirectional ion energy spectrogram, magnetic field, ion bulk velocity, ion density and current density deduced from the curlometer technique, respectively. At the start of the interval, B_x is negative and B_y is positive and energetic particles are observed in the ion spectrogram. This along with low ion density and low current density indicates that Cluster is sampling the magnetosphere. Around 06:42:30, there is a gradual change in all components of the magnetic field. B_x turned positive and B_z to negative, coinciding with the appearance of low energy ions, increased plasma velocity, sudden increase in the ion density as well as increased current density, indicating the first magnetopause crossing of the presented interval. Around 06:44:50, Cluster exits from the magnetosheath back into the magnetosphere. Again around 06:46:20 and 06:48:00, Cluster enters and exits the magnetosheath. Since from the two presented crossings into the magnetosheath, the latter includes a sharper and unstructured magnetic field signature and the current density incorporates an intense duskward component consistent with the large-scale Chapman-Ferraro current within the crossing area, we choose this crossing for further analysis in this paper in section 4.

3. Magnetopause Orientation and Speed

[16] The polar plots presented in Figure 3 show a comparison of the magnetopause normals obtained from CVA and COM methods. In both panels the bull's eye is the magnetopause orientation deduced from CVA method and each triangle corresponds to the COM normal of each magnetopause crossing, projected onto the plane defined by the bull's eye normal. The radial circles represent cones with equal inclination from the bull's eye. For each crossing, the directions of horizontal and vertical axes are independently defined by the bull's eye normal. For example, at subsolar point the normal would be in the sunward direction, then the axes would roughly be the GSE y and z. The radial distance between the triangle and bull's eye shows the angle between the normals from CVA and COM methods.

[17] Figure 3a shows results when no constraint is applied on the single-spacecraft analysis in deducing the COM method. For all the crossings, the COM normals are within 30 degrees from the CVA normals but for most of the crossings, the COM normals are within 10 degrees from the CVA normal, indicating that the COM is a good representation of the normals obtained by applying the GRA on the four conservation laws used to deduce the COM results. Normals from both CVA and COM that are very close to each other are generally required, while definition of a good separation depends on the application. In the two crossings that fall outside the 20 degree circle in Figure 3, the time period of the crossing is disturbed by near simultaneous other crossings affecting the quality of the CVA normal in the bull's eye. Furthermore, in both cases the MVAB applied to data from all Cluster spacecraft yields similar results for the magnetopause orientation, and hence the CVA normal in the two cases is possibly not reliable. For one third of the crossings, MVAB and MFR methods yielded similar orientations which are different to MMR and MER results. Due to the large eigenvalue ratios from MVAB and MFR, the COM is dominated by these two methods. This is commonly observed for crossings in which magnetopause signatures in the magnetic field and plasma data do not coincide temporally. Since the data interval is centered on magnetic field signature, the methods that use only plasma data yield different results to others.

[18] Figure 3b shows the results when a tangential discontinuity constraint is applied on the single-spacecraft methods. The different constraints that can be applied with the generic residue method are given by *Sonnerup et al.* [2006]. In this study we used the constraint $\langle \mathbf{B} \rangle \cdot \mathbf{n} = 0$, i.e. the average magnetic field along the normal is assumed zero. Except for six crossings, COM normals are within 20 degrees from the bull's eye. The normals are more widely separated as compared to the unconstrained analysis shown in Figure 3a.

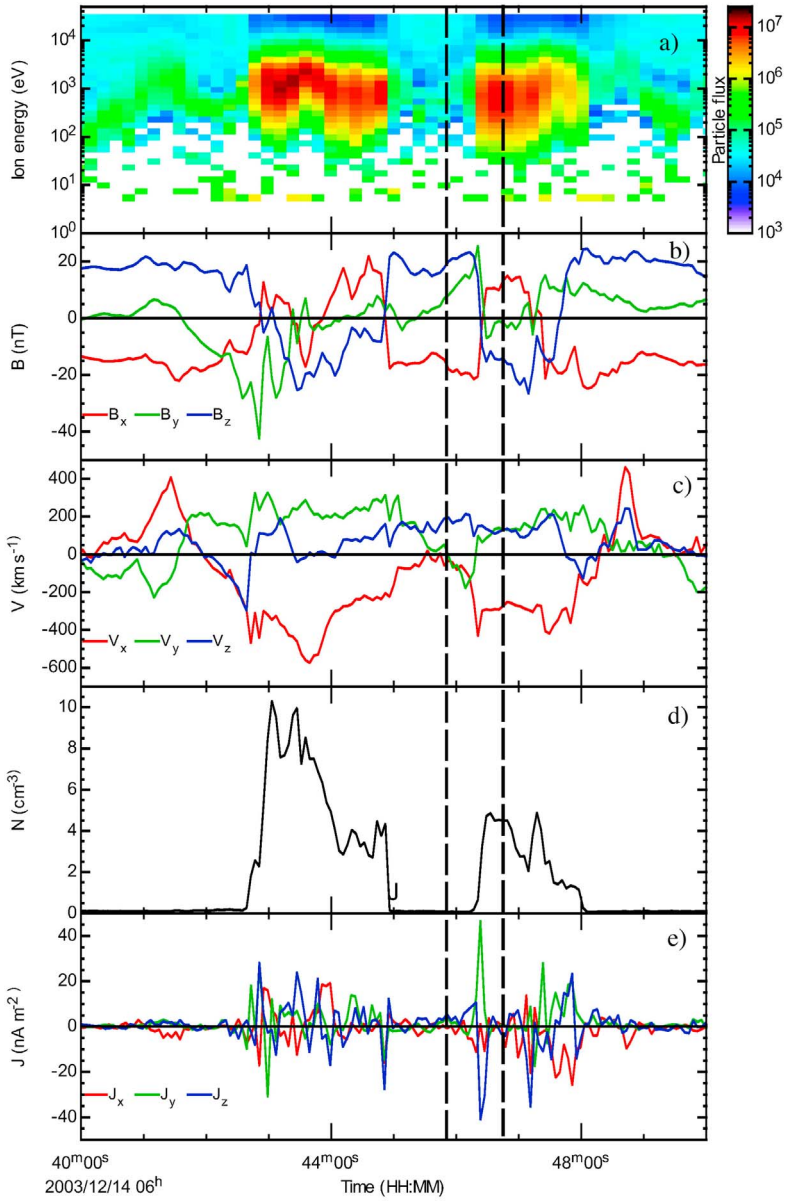

Figure 2. Cluster spacecraft 1 measurements on 14 December, 2003 on an outbound crossing. Shown here are (a) omnidirectional ion energy spectrogram, (b) magnetic field, (c) ion bulk velocity, (d) ion density, and (e) current density estimated using the curlometer technique. The two vertical dashed lines indicate the time period of the magnetopause crossing examined in this paper.

We suspect this is due to the presence of small but significant average normal component in the magnetic field during the crossings. The event with the largest separation between the COM and CVA (56 degrees, which falls outside the plot axes) occurs on 2002-05-10 (not shown in the plot), during which the average normal component in the magnetic field is large, violating the tangential discontinuity assumption.

[19] Figure 4 shows a comparison of the magnetopause velocities in the normal direction, deduced from COM and CVA methods. A positive (negative) velocity means that the spacecraft observes an outward (inward) moving magnetopause. Velocities from the CVA method ($V_{mp,CVA}$) are plotted along the x-axis, while the COM method velocities ($V_{mp,GRA}$) are plotted along the y-axis. Squares present a comparison of CVA velocities against COM velocities with no constraints applied on the COM method, and the dotted line is the linear fit. A correlation coefficient of 0.78 indicates a good correlation between magnetopause velocities estimated using CVA and COM. The inverted triangles show the comparison between the velocities deduced using the CVA method and constrained COM method, while the solid line is the linear fit. A correlation coefficient of 0.71 indicates that the quality of the constrained normals also affects the quality of the magnetopause velocity. A slope of 0.71 and 0.78 indicate a systematic difference of CVA and the COM methods. We note that CVA will only give reliable results if the discontinuity is

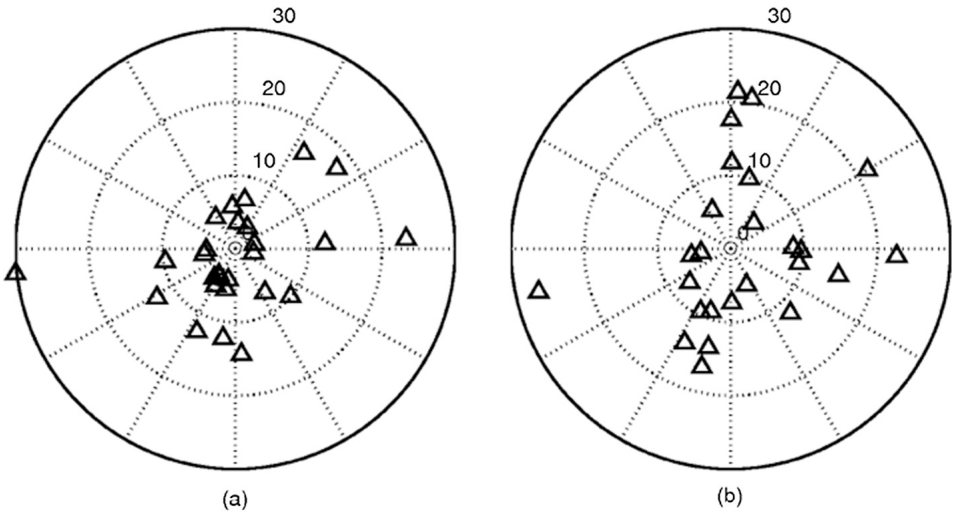

Figure 3. Polar plots showing a comparison of the orientation of the magnetopause obtained from COM and CVA methods. The position along the radial direction gives the angular separation between the normals being compared and azimuthal direction is the plane perpendicular to the reference normal given by the bull's eye. For example, at subsolar point the normal would be in the sunward direction, then the axes would roughly be the GSE y and z. In both panels, the bull's eye is the orientation provided by the CVA method and the triangles are individual magnetopause crossings. (a) Results without the use of constraints on COM and (b) results when tangential discontinuity constraint, i.e., $\langle \mathbf{B} \rangle \cdot \mathbf{n} = 0$ is applied on COM.

planar and has no acceleration. However, during some of the magnetopause crossings presented in this paper we suspect the presence of an acceleration of the magnetopause supported by the observation of multiple crossing and this possibly explains the discrepancy. However, most importantly, both methods yield velocities with similar signs; if one of the two methods results in opposite sign for the velocity, it will

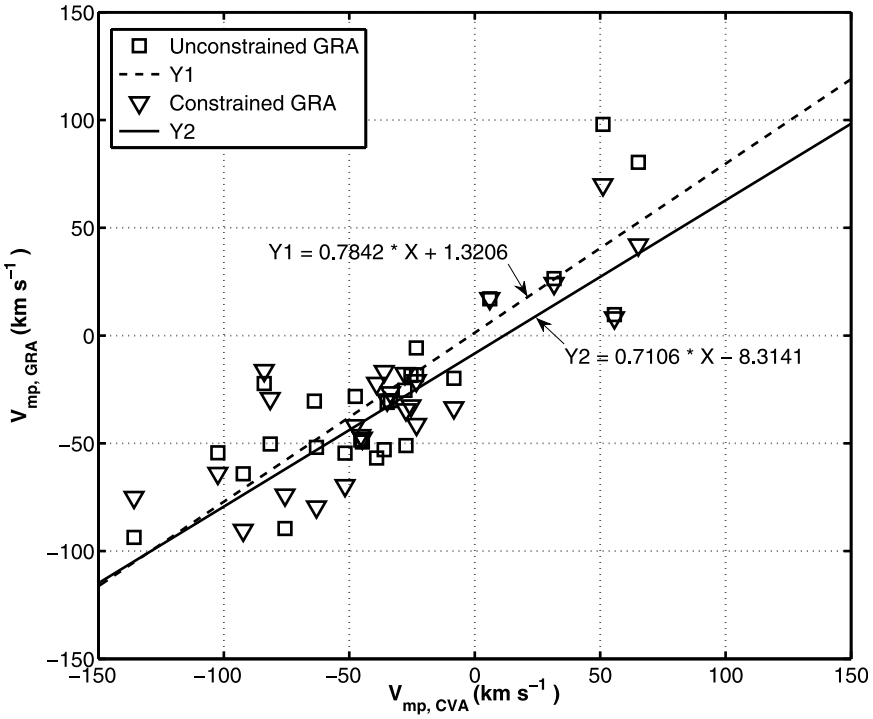

Figure 4. Comparison of the magnetopause velocity along the normal from CVA and COM. Positive/negative sign indicates an outward/inward moving magnetopause from the Earth. Squares represent a comparison of CVA results against unconstrained COM and the dashed line is a linear fit. Triangles shows a comparison between CVA against COM with the tangential discontinuity constraint, i.e., $\langle \mathbf{B} \rangle \cdot \mathbf{n} = 0$ and the bold line is the corresponding linear fit.

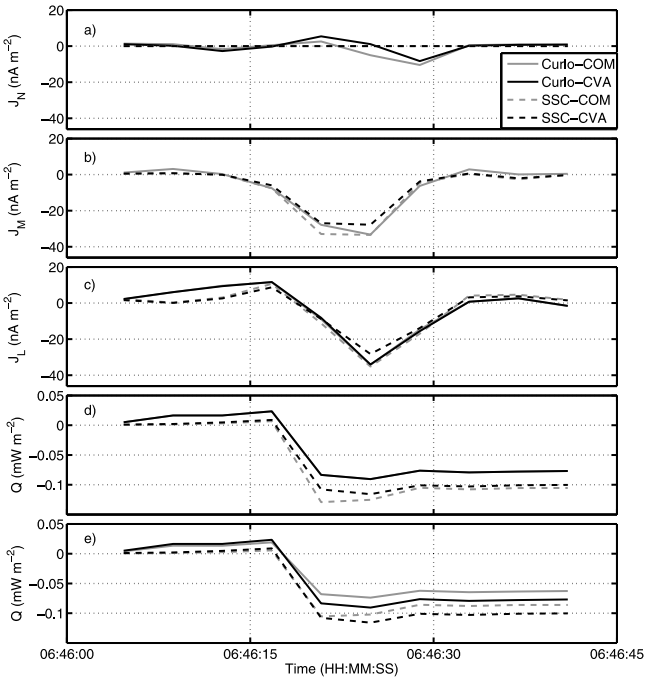

Figure 5. Estimated current density and energy conversion during a magnetopause crossing on Dec 14, 2003 using multi and single-spacecraft methods. The black (gray) curves are in boundary normal frame determined by CVA (COM) method, whereas the solid (dashed) lines are currents estimated using curlometer (single-spacecraft) method. (a–c) The N, M and L components of the current density, respectively. (d and e) The estimated energy conversion using curlometer (solid lines) and single-spacecraft currents (dashed lines) in CVA (black lines) and COM frames (gray lines). All the curves represented in Figure 5d use same magnetopause velocity (from CVA, 135.8 km/s) in energy conversion estimation whereas the black (gray) lines in Figure 5e use the magnetopause velocity given by CVA (COM) methods.

influence the single-spacecraft current density and consequently the sign of the energy conversion estimate.

4. Energy Conversion at the Magnetopause

[20] Here we compute the energy conversion estimated during a magnetopause crossing on Dec 14, 2003, shown in Figure 2, using both single and multispacecraft techniques. For this crossing, the magnetopause normal given by CVA is [0.81, 0.51, 0.31] and COM is [0.80, 0.27, 0.53] in GSE. These two normals are separated by 17 degrees, while the velocity of the magnetopause deduced from CVA is −135.8 km/s and −91.5 km/s from COM. The results from COM are dominated by MVAB method having a weight of 0.87, while other methods have smaller weights. However, MVAB and MFR frames include an average normal magnetic field of 0.28 nT and 2.66 nT, respectively, whereas MMR and MER frames include a large normal magnetic field component of ~6 nT. Hence, for this crossing, we estimated the COM normal using only MVAB and MFR methods, which decreased the angular difference with respect to CVA to 8 degrees and brought the magnetopause velocity to −110.8 km/s. Hence, we use only deHoffmann-Teller frame velocity [*de Hoffmann and Teller*, 1950] along the normal from MVAB and MFR to deduce COM in further analysis of this event.

[21] Figure 5 demonstrates the effect of the magnetopause orientation, speed along the normal and current density on the energy conversion estimation using equation (1). Figures 5a–5c show the current density components estimated using curlometer (solid lines) as well as the single-spacecraft method (dashed lines). The black (gray) lines are in the CVA (COM) boundary normal frame. The normal component of the current density from the single-spacecraft method is zero, while from curlometer the average normal component over the plotted period is −0.17 nAm^{-2} and −0.84 nAm^{-2}, in COM and CVA frames, respectively. The M and L components of current density from single-spacecraft and curlometer in CVA and COM frames (Figures 5b and 5c) are in quantitative agreement.

[22] Figures 5d and 5e show energy conversion estimates using the current densities shown in Figures 5a–5c, where again the black lines are in CVA frame and gray are in COM frame. The solid lines are the energy conversion estimates using current density from curlometer using the CVA and COM frames, whereas the dashed lines are those for which single-spacecraft current estimates are used, from the two frames. To demonstrate the effect of the current density and the normal orientation, in Figure 5d we compute the energy conversion using magnetopause velocity predicted by CVA method in the integration. The two solid lines having different frames but the same values for current and magnetopause velocity are overlaid on one another. This is due to the fact that the scalar triple product is invariant of the coordinate system, and any difference in energy conversion calculated in two different boundary normal frames will be due to the difference in the magnetopause velocities given in those frames. The dashed lines represent energy conversion estimates using the single-spacecraft current density in both CVA (black) and COM (gray) frames, again having the same velocity of the magnetopause. Hence, the small magnitude difference among the dashed lines is due to the 7 degree angular difference between the two normals. Figure 5d indicates that the single-spacecraft estimates of the Q are slightly larger than those computed with curlometer current density. This difference is due to the difference in normal orientation and in the lack of normal current component in the single-spacecraft energy conversion estimates.

[23] Figure 5e is similar to Figure 5d except that here we used the V_{mp} deduced from CVA (black lines) and COM (gray lines) methods in energy conversion estimates instead of using the same value for the magnetopause velocity. Now the magnitude difference between the energy conversion using curlometer current in CVA and COM frames (solid lines) is only due to the difference between the V_{mp} in the two frames, while the magnitude differences among the energy conversion estimates using single-spacecraft current in CVA and COM frames also include the effect of the differences between curlometer current density and single-spacecraft current density. We conclude that in a clear and unstructured crossing such as the one presented here(cf. Figure 2), uncertainties related to orientation and current density are relatively small, around 25% from each other.

[24] In Figure 6, we demonstrate the importance of choosing the time interval to estimate the energy conversion across the magnetopause. Shown in Figures 6a–6d are the magnetic field, plasma velocity, current density from curlometer and from

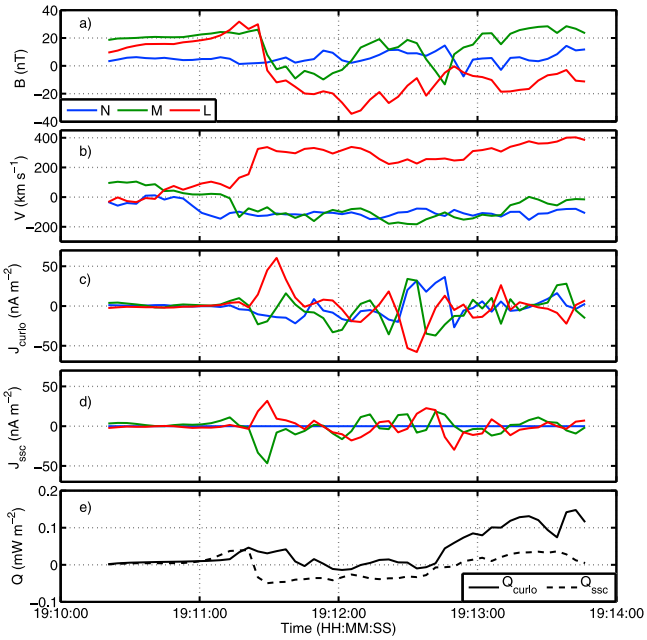

Figure 6. A magnetopause crossing on Jan 18, 2004: (a–d) magnetic field, plasma velocity, curlometer current density and the single-spacecraft current density, respectively. All the quantities are in LMN frame given by the CVA method. (e) The energy conversion estimates with curlometer current (solid line) and with single-spacecraft current (dashed line).

single-spacecraft, respectively, during a dayside magnetopause crossing on Jan 18, 2004. All the quantities are LMN components computed in the CVA frame. Figure 6e shows the estimated energy conversion using curlometer current (solid line) and the single-spacecraft current (dashed line). The magnetopause crossing is shown by a clear change in the L-component of the magnetic field and plasma velocity around 19:11:20 UT during which current densities from both the curlometer and single-spacecraft show a strong enhancement. The negative M-component of the current density indicates a duskward large-scale Chapman-Ferraro current direction on the dayside equatorward of the cusp.

[25] Figures 6c and 6d indicate that the current density is highly fluctuating after the actual magnetopause crossing at 19:11:20 UT. These fluctuations include both positive and negative values in the M-component, and a large normal component in the curlometer estimate. Clearly these fluctuations are not associated with a magnetopause current layer crossing, because the plasma density does not show a marked change and the magnetic field proxies are not as clear as at 19:11:20 IT. As shown by *Palmroth et al.* [2011], the current density can show fluctuations that are associated with boundary layer dynamics. Figure 6e shows that these fluctuations can deteriorate the energy conversion estimate, which is negative during the actual magnetopause crossing but becomes positive toward the end of the plotted period. Hence, the energy conversion can reflect local properties of the magnetopause, which calls for caution when interpreting the results.

[26] Next, we present an outbound magnetopause crossing within the dayside cusp region on Apr 06, 2004. Cluster exited the magnetosphere and entered the magnetosheath around 04:34:15 UT, when the CIS/HIA ion spectrogram (not shown) indicates a clear transition from a region populated by high energy ions to the cold and dense magnetosheath. For this crossing, the magnetopause normals provided by COM and CVA are [0.77, 0.38, 0.50] and [0.77, 0.44, 0.47], respectively, which fall within 2 degrees of each other. The magnetopause velocity is −62.9 km/s from COM and −47.6 km/s from CVA. The COM for this crossing is dominated by the MVAB, for which the ratio between the intermediate and minimum eigenvalues is largest (8), and consequently it also has the highest weight (87%). Furthermore, the average normal magnetic field components from COM and CVA are small (−1.47 *nT* and −0.68 *nT*, respectively), indicating that the results from COM and CVA are reliable.

[27] In Figure 7, we investigate the effect of the normal current density component on the energy conversion. Shown are the estimated current density and energy conversion during the Apr 06, 2004 crossing, again using multi and single-spacecraft methods. Figures 7a–7c show the N, M and L components of the magnetopause current density, respectively. The line types are similar to Figures 5a–5c. As seen in Figure 7a, the normal component of the current from curlometer is significant (+/−45 nAm^{-2}) and comparable in magnitude with the L-component. Hence, there is a significant difference between the curlometer current and the single-spacecraft estimate of the normal component, which is assumed zero. The M-component from curlometer and single-spacecraft techniques are in quantitative agreement. The M-components from both methods are strongest in the negative M-direction, consistent with the Chapman-Ferraro current equatorward of the cusp in the dayside magnetopause. The L-component from curlometer is larger compared to the L-component from the single-spacecraft method, especially within the strongest current sheet.

[28] Similar to Figure 5d, the solid (dashed) curves in Figures 7d–7f use curlometer (single-spacecraft) current, and the black (gray) curves are in CVA (COM) frame. Figure 7d, which is similar to Figure 5e, indicates that the energy conversion estimates using single and multispacecraft estimates are of different sign, regardless of the frame in which the computations are carried out. In Figures 7d–7f we investigate whether this is due to the large normal component produced by the curlometer technique. In Figure 7e, the dashed curve represents a case where the single-spacecraft normal current component, which is assumed zero in the technique, is replaced by the normal current component from the curlometer technique. In contrast in Figure 7f, the normal component from the curlometer technique is assumed zero. These replacements demonstrate the significance of the normal current component during the crossing. Figure 7e shows that when the curlometer normal component is used to estimate energy conversion using single-spacecraft methods, the final Q becomes negative. Instead, Figure 7f shows that if the normal current is assumed zero as is done in the single-spacecraft method, all the energy conversion estimates become positive. For a clock angle of 240 degrees, the simulation results from *Laitinen et al.* [2007] suggests a positive energy conversion at the position of Cluster crossing (X_{GSE} = +6.9R_E, Y_{GSE} = −1.3R_E and Z_{GSE} = +6.4R_E). Hence, here the large normal component in the curlometer current leads to sign ambiguity in the energy conversion.

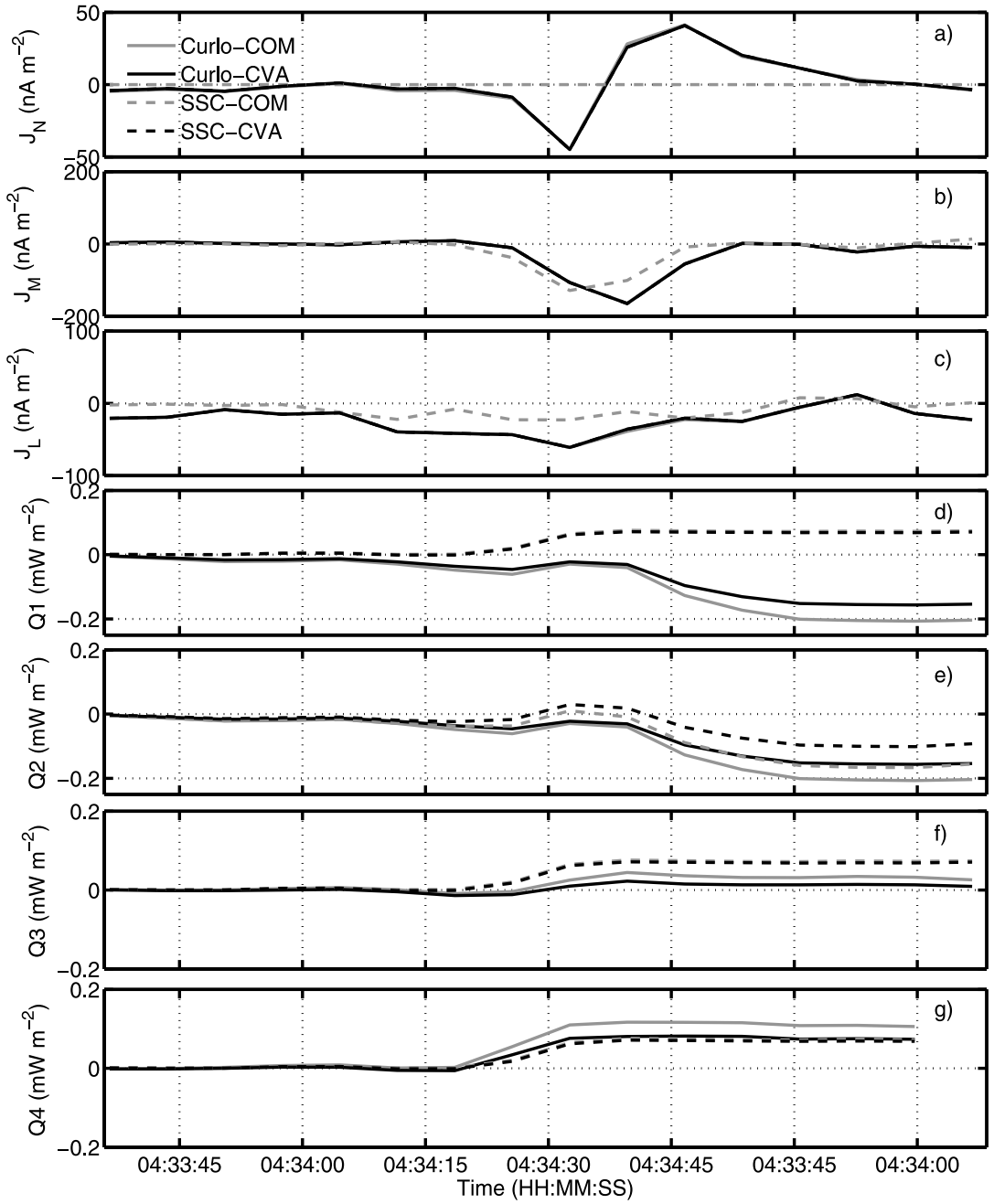

Figure 7. Current density and energy conversion during a magnetopause crossing on Apr 6, 2004, using multi and single-spacecraft methods. (a–c) The N, M and L components of magnetopause current density, respectively. The description and color coding are similar to Figures 5a–5c. (d–f) The energy conversion estimates using different values for the normal current. Figure 7d is similar to Figure 5e. In Figure 7e the solid lines use curlometer current in CVA (black) and COM (gray) frames and the dashed lines use single-spacecraft current after the normal current being replaced by the normal current from curlometer. In Figure 7f the dashed lines use the single-spacecraft current whereas the solid lines use the current from curlometer with zero normal current. (g) The energy conversion similar to Figure 7f but the curlometer current is moved backwards in time to match the peak of the major component of current (M) from the single-spacecraft method.

[29] The curlometer gives an estimation of the current density at a virtual spacecraft in the center of the tetrahedron, whereas the SSC gives the current profile in the corner of the tetrahedron as detected by the selected spacecraft. This may lead to a time offset of a few seconds among the current estimated at the center and corners of the tetrahedron. For all the events used in this study we have checked this time offset and corrected wherever needed. Figure 7b shows that the minimum curlometer current does not appear simultaneously with the minimum of the single-spacecraft current.

Table 1. Summary of All the Magnetopause Crossings Used in This Study[a]

Date	Time Interval	Sign Difference	Cause	θ_{IMF}	Q_{ssc} (μWm^{-2})	Q_{multi} (μWm^{-2})	$\frac{\nabla\cdot\mathbf{B}}{\lvert\nabla\times\mathbf{B}\rvert}$ (%)
20020203	09:14:24 - 09:15:28	No	None	290	22.30	84.50	32.26
20020206	08:16:03 - 08:18:11	No	None	76	20.60	19.80	28.67
20020218	04:59:11 - 05:00:11	No	None	280	−4.55	−116.00	36.52
20020302	03:30:43 - 03:31:32	Yes	Time offset	57	−9.47	−14.30	38.45
20020330	13:27:38 - 13:29:38	No	None	125	−150.00	−135.00	49.24
20020410	23:10:32 - 23:11:12	No	None	60	39.60	26.30	36.76
20020423	08:15:01 - 08:19:30	Yes	Both	90	−150	−325.00	41.59
20020510	04:26:00 - 04:27:21	Yes	J_N	250	−0.35	−22.00	32.54
20020521	22:07:00 - 22:07:56	Yes	J_N	50	18.00	147.00	34.53
20020605	08:31:56 - 08:34:28	No	None	350	23.60	123.00	20.70
20020607	17:42:02 - 17:44:07	No	None	250	−11.50	−16.10	41.22
20020613	19:00:33 - 19:01:46	No	None	205	−5.87	−47.10	32.09
20020616	00:55:03 - 00:55:47	No	None	No data	−16.60	−9.23	40.82
20031125	11:42:47 - 11:43:27	No	None	175	25.50	21.40	38.56
20031201[b]	13:08:19 - 13:09:27	No	None	100	-	-	54.78
20031214	06:46:00 - 06:46:40	No	None	240	−56.40	−76.50	41.07
20040104	14:10:16 - 14:13:42	No	None	350	−72.40	−230.00	32.24
20040118	19:10:16 - 19:12:17	Yes	Both	0	−38.50	−14.90	36.60
20040128	06:36:03 - 06:37:52	No	None	110	12.70	16.60	26.67
20040130	16:56:02 - 16:57:55	Yes	Both	90	−14.00	−17.20	20.97
20040221	01:20:50 - 01:22:51	No	None	300	6.43	3.38	17.35
20040228	04:01:00 - 04:04:02	No	None	140	88.20	279.00	42.17
20040229[b]	23:00:28 - 23:01:16	No	None	No data	-	-	156.8
20040306	08:33:30 - 08:37:00	Yes	J_N	135	43.00	58.20	36.91
20040406	04:33:48 - 04:34:48	Yes	Both	250	74.40	15.90	40.55
20040410	22:43:00 - 22:44:29	Yes	Both	250	−35.70	−19.90	26.56
20040415	16:32:19 - 16:32:59	No	Time offset	250	18.20	36.50	43.05

[a]Time interval is the interval used to calculate the energy conversion from multispacecraft method (Q_{multi}) and single-spacecraft method (Q_{ssc}). Sign difference column tells whether there was a sign difference between the two estimates before the sources of error in section 4.1 were taken into account. The cause for ambiguous signs in estimated energy conversion is presented in the fourth column. The last column shows the quality of curlometer as percentage.

[b]During these events, the curlometer current is not reliable as the measure of quality of curlometer is more than 50% and we have not considered them in energy conversion calculations and do not form part of energy conversion statistics.

In Figure 7g, we investigate the effect of this offset at the time of minimum in the major current component. Figure 7g shows the energy conversion similar to Figure 7f, but now the curlometer current is moved 4 s backward in time and the normal current is kept zero. This correction brings the final energy conversion estimates using different methods closer to each other. The offset in minimum times of the major component in the current from the two methods can hence lead to a difference in the estimated energy conversion magnitude. However, our database includes cases where this offset alone can result in ambiguity in the sign of the energy conversion.

5. Statistical Analysis

[30] Table 1 shows a summary of the estimated energy conversion for all the magnetopause crossings analyzed in this study. A total of four different estimates of energy conversion are introduced: Energy conversion calculated using curlometer (Curlo) current in COM and CVA frames ($Q_{Curlo-COM}$, $Q_{Curlo-CVA}$) and the energy conversion calculated using single-spacecraft current (SSC) in COM and CVA frames ($Q_{SSC-COM}$, $Q_{SSC-CVA}$). The four estimates agreed in sign during most of the crossings, while the magnitude differences is due to the ambiguities introduced by different parameters used to calculate equation (1). The third column of Table 1 specifies whether there was a sign difference, while the fourth column indicates the cause for the difference. IMF clock angle and the energy conversion estimate from single-spacecraft techniques i.e., using single-spacecraft current in COM frame, is shown in fifth and sixth columns, respectively. The seventh column shows the energy conversion estimated using multispacecraft techniques i.e., using curlometer current in CVA frame and the last columns shows the percentage of ratio between the divergence of magnetic field to the curl of magnetic field. This is a measure of the quality of the curlometer current. Since some events included ambiguity in the sign of the energy conversion estimate, we applied in those events corrections to arrive in a consistent sign for all four estimates. The corrections are outlined in Section 4, and they include the shift of the curlometer current density to match the temporal evolution of the single-spacecraft current, taking into account only the Chapman-Ferraro current system (time interval of the crossing), and considering the unrealistically large current normal component in curlometer. The corrected value is verified against the GUMICS-4 simulation result within the area of the Cluster crossing.

[31] Figure 8 presents histograms of differences between the four estimates both in the uncorrected database (gray) as well as after corrections in the few events where the four estimates yielded inconsistent sign for the energy conversion (black). The y-axis in all panels show the number of crossings in each bin. The x-axis in Figures 8a and 8b shows the difference between Q using SSC in COM and CVA frame normalized to $Q_{Curlo-COM}$ and $Q_{Curlo-CVA}$, respectively. Figures 8a and 8b illustrate the uncertainty caused by the use of single-spacecraft current in COM and CVA frames, respectively. Before applying the corrections, one fourth of the events have more than 100% uncertainty, whereas after the corrections most of the events fall within 100% uncer-

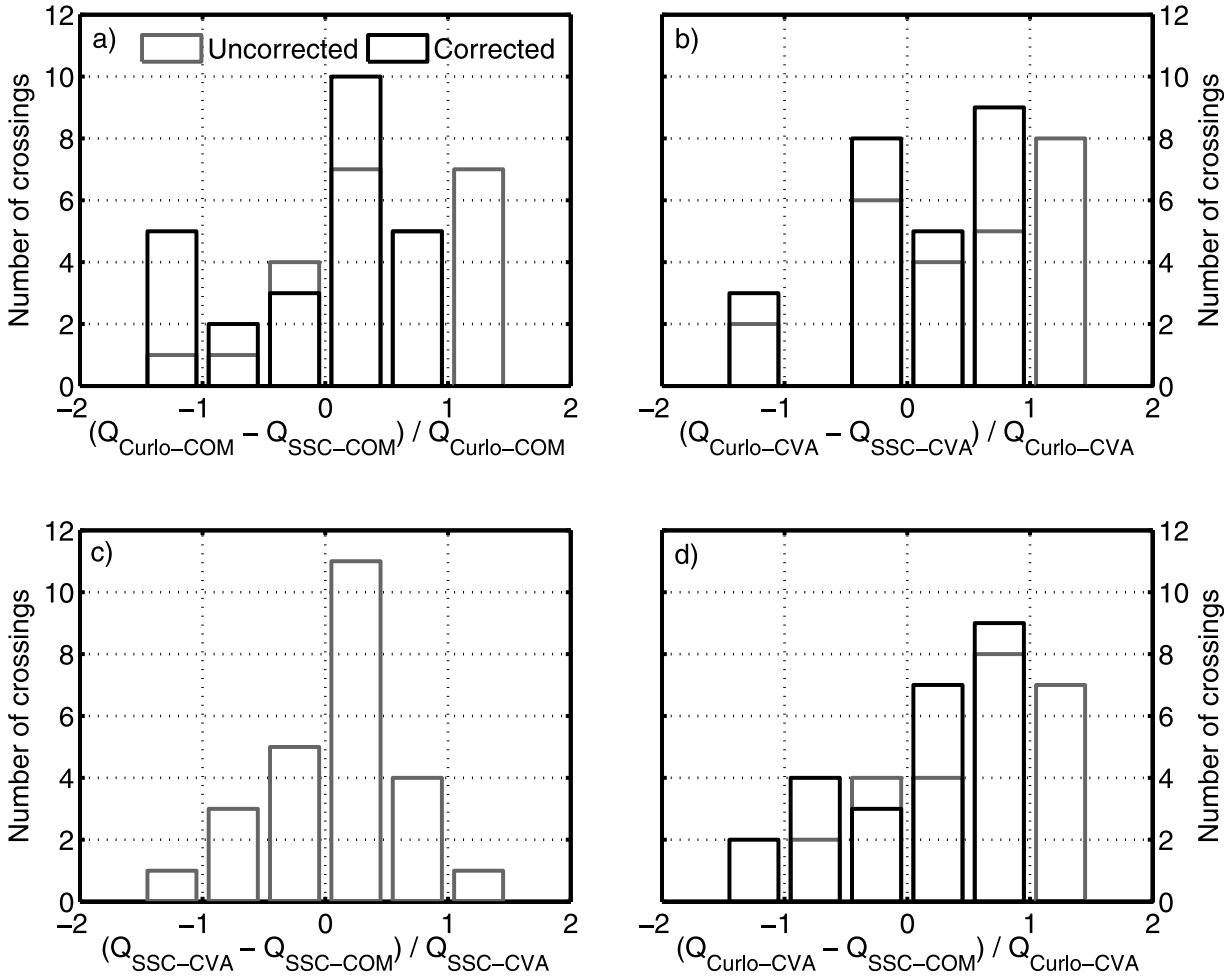

Figure 8. Statistical nature of the errors introduced by the use of single-spacecraft methods. Black (gray) lines represent energy conversion results using the corrected (uncorrected) curlometer current. (a and b) The statistics of the ambiguities introduced by the use of single-spacecraft current approximation in COM and CVA frames, respectively. (c) Statistical representation of the ambiguities introduced due to the separation between normals from the two methods; (d) the combined effect of all the ambiguities introduced by the normal, single-spacecraft current and the magnetopause velocity.

tainty. In Figure 8c, the x-axis shows the difference between Q_{SSC} in COM and CVA frames and normalized to $Q_{SSC\text{-}CVA}$, highlighting the ambiguity introduced due to the separation between the normals from COM and CVA methods. Most of the events are within +/−50% uncertainty level. In Figure 8d, the x-axis shows the difference between multispacecraft estimate ($Q_{Curlo-CVA}$) and the single-spacecraft estimate ($Q_{SSC-COM}$) and is normalized to $Q_{Curlo-CVA}$, and demonstrates the ambiguities due to the separation between normals, SSC and magnetopause velocity (V_{mp}). Again after corrections, the uncertainty is within +/−100%.

[32] In Figure 9, we demonstrate the ambiguities introduced by different quantities in estimating Q. The grey (black) squares are estimates before (after) the corrections are applied to remove the sign ambiguities. In Figure 9a we examine the effect of the use of SSC to estimate Q in COM frame compared with $Q_{Curlo-COM}$. Before the corrections, there are a few events with sign ambiguities which lead to poor correlation while the slope and correlation coefficient improve after the corrections removing the sign ambiguity. From the linear fit to the corrected values it is clear that the Q using the SSC is lower than using Curlometer current by about 50%. Figure 9b examines the effect of SSC on Q estimated in the CVA frame. Again the corrections lead to a better correlation coefficient and the Q using SSC is lower than using Curlometer current by ~35%. In Figure 9c we examine the effect of the separation of the different frames on Q. Plotted are the Q using SSC in CVA (along horizontal axis) and COM (along vertical axis). The linear fit to the data indicates again that Q in COM using SSC is lower by 50% compared to Q using SSC in CVA frame, while the same sign is retained. Figure 9d shows multispacecraft estimate ($Q_{Curlo-CVA}$) against the single-spacecraft estimate ($Q_{SSC-COM}$). Figure 9d shows that when all the ambiguity sources are present, the single-spacecraft estimate is lower by two thirds compared to the multispacecraft estimate.

[33] In Figure 10, we present the statistical uncertainties of $Q_{SSC-COM}$ and compare to $Q_{SSC-CVA}$ and $Q_{Curlo-CVA}$. Appendix A shows the details of the uncertainty calculation in COM frame. In both panels, horizontal axis shows the

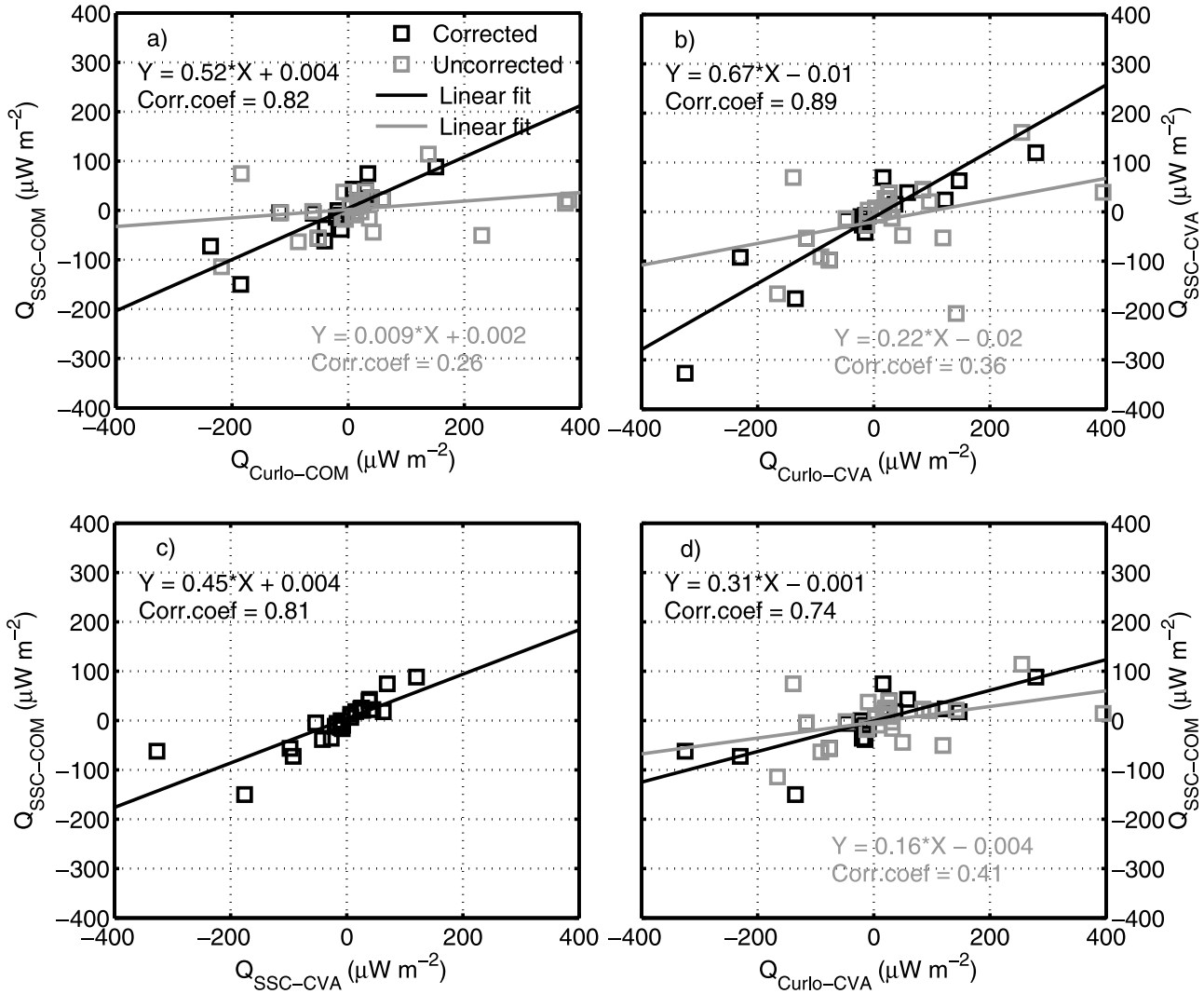

Figure 9. Demonstration of differences in energy conversion using the currents from curlometer and single-spacecraft and in multispacecraft (CVA) and single-spacecraft (COM) frames. (a) The Q using single-spacecraft and curlometer current in COM frame. (b) Q in CVA frame. (c) Q using single-spacecraft current in CVA and COM frames. (d) Q using single-spacecraft and multispacecraft methods.

number of the event and the vertical axis shows the energy conversion magnitude. The gray squares are $Q_{SSC-COM}$ along with the uncertainty estimates depicted with error bars. Figure 10a shows a comparison of $Q_{SSC-COM}$ against $Q_{SSC-CVA}$ (black squares). Clearly for most of the cases $Q_{SSC-CVA}$ is within the uncertainty limits of $Q_{SSC-COM}$. The comparison is similar to Figure 9c, where the differences are due to the angular difference in the normals from COM and CVA. In Figure 10b we present $Q_{SSC-COM}$ and the uncertainties (grey) compared to $Q_{Curlo-CVA}$ (black squares). Again, for most of the crossings, $Q_{SSC-COM}$ is comparable to $Q_{Curlo-CVA}$ if the uncertainty estimates are taken into account.

6. Discussion

[34] In this paper we have presented a small statistical study of energy conversion at the magnetopause following the methodology of *Rosenqvist et al.* [2006, 2008a, 2008b]. To limit the number of possible sources of errors in the analysis, we use a previously published data set [*Panov et al.*, 2008], where the quality of the magnetopause crossings is controlled and the multispacecraft methods can be used and validated against the published values. While the multispacecraft methods are generally believed to yield best results [*Dunlop et al.*, 2006; *Haaland et al.*, 2006], a large statistical study cannot be planned to depend on the multispacecraft methods. This is mainly because the multispacecraft method for the current density, the curlometer technique, gives best results with a small spacecraft separation, limiting the number of events that can be used in the analysis due to the Cluster separation strategy. Hence any statistical study aimed at estimating energy conversion at the magnetopause in the large scale requires the use of single-spacecraft data and methods. In this paper, our main goal is to compare the energy conversion estimated using the single-spacecraft techniques against the multispacecraft techniques. For multispacecraft methods, we use the Constant Velocity Approach (CVA) and the curlometer technique, while the Generic Residue Analysis

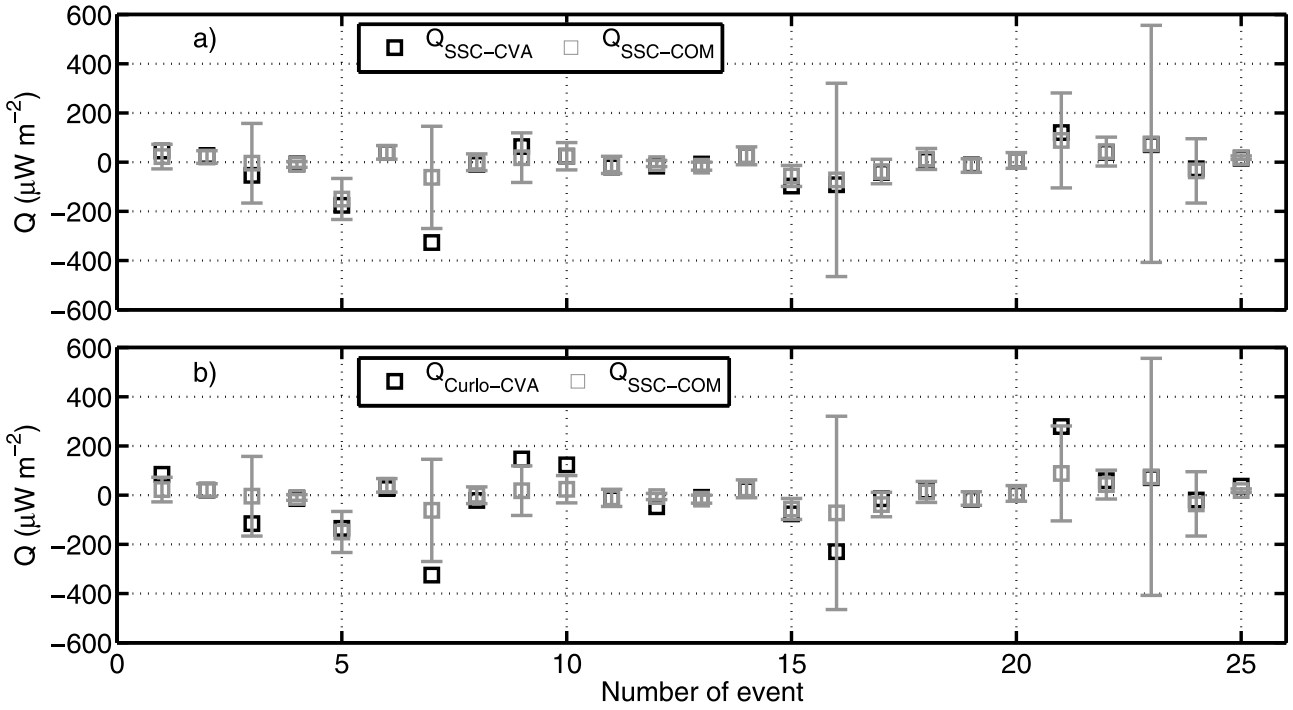

Figure 10. Demonstration of the uncertainties in the energy conversion estimates from single-spacecraft methods. (a and b) Gray squares with error bars represent the energy conversion and their associated uncertainties from single-spacecraft current in the COM frame. The black squares in Figure 10a (Figure 10b) are energy conversion estimates using single-spacecraft (curlometer) current in CVA frame.

(GRA) and a standard one-dimensional current estimation is used for single-spacecraft methods.

[35] The first finding in this paper is that the evaluation of Q using equation (1) yields ambiguous results during some events when using different methods to estimate the required variables. The determination of the magnetopause speed, which is a constant multiplier in equation (1) depends on the orientation of the magnetopause, and hence it can have a large effect on the results. Figure 4 suggests that single-spacecraft V_{mp} determination is lower by 20%, bringing the same multiplier in the final Q. The comparison of magnetopause normals in Figure 3 suggests that for most of the crossings, both unconstrained and constrained COM normals are within 20 degrees of the CVA normals, but the constrained normals are more spread around the CVA normal. The previous work by *Haaland et al.* [2004] showed that using constraints on single-spacecraft methods results in a better normal during the analyzed event. This inconsistency is possibly due to the nature of the events here, where a normal magnetic field component is present, indicating reconnection and an open magnetopause or possibly the magnetopause acceleration. Furthermore, the results and the differences between the COM and CVA methods are explained by a number of factors: model assumptions (planarity, 1D, no acceleration etc.), data (quality of higher order plasma moments in GRA, possible offsets in the magnetic field) application (selecting time intervals, center times, determining crossing times, window sizes). *Haaland et al.* [2004] and *Sonnerup et al.* [2006] compared the multispacecraft normals and single-spacecraft normals against a normal obtained by averaging the normals obtained from four Cluster spacecraft using constrained MVAB. In this paper we are comparing COM normals against CVA normal instead, which may also explain some of the variability in the results. Most importantly, in light of the energy conversion at the magnetopause, we find that the separation between the magnetopause normals from the two methods affect the magnetopause velocity and the single-spacecraft current estimation, introducing ambiguities in the energy conversion calculation from COM method compared with CVA method. These ambiguities are of the order of 50%.

[36] Four different estimations of the energy conversion gives an opportunity to investigate how the final result depends on the different methods. The second important finding in this paper is that the different methods used to infer the energy conversion may yield a different sign for the final result. Hence, in a large statistics, a positive value indicating a "load" in the energy conversion system could appear in the tail lobes that should show a negative value indicating a "generator". As also suggested by *Palmroth et al.* [2011], the selection of the time interval of the magnetopause crossing is important, because local current systems not associated with the large scale Chapman-Ferraro system may also introduce sign differences. In Table 1 the "Sign difference" column indicates whether there is a sign difference between the multi and single-spacecraft estimates. If there is a sign difference ("Yes"), the "Cause" column shows the potential cause of the sign difference. We have identified two causes for the sign flip, both associated with the determination of the current density. First, an offset in the time of the curlometer current maximum or minimum compared to the single-spacecraft current may cause the sign flip in the final result. The reason for the time offset is that the curlometer gives an estimation of

the current density at a virtual spacecraft in the center of the tetrahedron, whereas the SSC gives the current profile in the corner of the tetrahedron as detected by the selected SC. The time offset will be a difficult question in the final large statistics because it requires a manual correction. Secondly, in some cases marked as having J_N in Table 1, the normal current from curlometer is large. This may introduce a sign flip as well, because the normal current is set to zero in the single-spacecraft methods. Furthermore, one does not expect a large normal component in current density at the magnetopause unless it is a crossing in the vicinity of the cusps. One more possibility is the presence of surface waves on the magnetopause, which may distort the magnetopause orientation and result in erroneous normal current. Both the large normal current or the time offset of the current maximum/minimum can cause the sign flip alone, but if the two effects appear together, also the magnitude of the energy conversion may have ambiguities.

[37] In this paper we have assumed that when all four methods to infer the energy conversion yield the same sign, which is also consistent with our global MHD simulation GUMICS-4 at the location of the Cluster crossing during similar upstream condition, we have arrived to the right sign of the energy conversion. This introduces the opportunity to correct the sign by taking into account only the Chapman-Ferraro current layer, by moving the curlometer current by one spin period, or by neglecting the normal current. These corrections are demonstrated in Figure 9. For the corrected results in Figures 9a and 9b, the only difference in the quantities is the estimation method of the current density. In the COM frame the single-spacecraft current introduces an ambiguity of 50% where as in CVA frame it is only 35%. This indicates that for most of the crossings the CVA estimation yields more accurate orientations compared to the COM normals. However, Figure 9 indicates that the COM normals are still usable in determining the energy conversion, giving hope for the final large statistics. Furthermore, even using CVA, there is still an ambiguity of 35% arising from the current densities, indicating that the method for inferring the energy conversion using single-spacecraft current will always have an uncertainty compared to that using curlometer current.

[38] To summarize the ambiguities introduced by all the contributing quantities, we note that on average the single-spacecraft methods introduce ambiguities of around 50%, 25% and 20% due to the current estimation, normal direction and velocity of the magnetopause, respectively, compared to the multispacecraft estimate. A contribution of 50% to the ambiguity from single-spacecraft current also contains the influence of normal direction indirectly. Hence we estimate an average ambiguity of around 70% in the energy conversion estimate from single-spacecraft methods. Also Figure 9d suggests that the single-spacecraft results are 70% smaller than the multispacecraft results.

[39] It is generally believed that the multispacecraft methods yield better results, given the suitable conditions for the applicability of those methods. In this study we have applied Curlometer and CVA methods to magnetopause crossings with inter-spacecraft separation of 100–200 km, which is suitable for the application of these methods. Here the $Q_{Curlo\text{-}CVA}$ is considered *a priori* as the reference estimate of energy conversion. Figure 10 shows that the uncertainties are small for most of the cases and the reference estimate is within the uncertainty of the single spacecraft estimate, and hence the choice of reference is a matter of opinion in many cases. We conclude that the choice of the reference here is supported by the single spacecraft method as well, and that the energy conversion is accurately estimated in this paper. However, we do not rule out the possible breakdown of the planar magnetopause assumption, in which case the single-spacecraft methods, although correct, pick up smaller scales than the inter spacecraft separation scale. This leads to differences between the single-spacecraft and multispacecraft energy conversion results. This may be a reason for large magnitude differences seen in Figure 10b during few crossings.

7. Summary

[40] We have investigated the magnetopause energy conversion using the Cluster observations, both with single and multispacecraft methods. The main results of this paper are the following.

[41] 1. Single-spacecraft results are generally consistent with multispacecraft methods, although they give lower values compared to the multispacecraft methods.

[42] 2. The uncertainties in single-spacecraft methods are generally small and the energy conversion estimates from single-spacecraft are consistent with multispacecraft estimates when the uncertainties are considered.

[43] 3. For majority of the crossings, the obtained energy conversion rates are in the range (1–100 μW m^{-2}), consistent with previous observations [*Rosenqvist et al.*, 2006] and with simulations [*Palmroth et al.*, 2011].

[44] 4. Single-spacecraft estimate yielded ambiguities of around 50%, 25% and 20% due to the current estimation, normal direction and velocity of the magnetopause, respectively, compared to the multispacecraft estimate.

[45] 5. In some cases, the single-spacecraft methods yield a different sign for the energy conversion compared to the multispacecraft methods. These sign ambiguities arise from the orientation of the magnetopause, choosing the interval to be analyzed, large normal current and time offset between the single spacecraft and multispacecraft methods.

Appendix A

[46] In this study we have calculated the statistical errors in the single-spacecraft method (COM) using the equations presented by *Sonnerup and Scheible* [1998]. The angular uncertainty in the estimation of eigenvectors, expressed in radians, is given as

$$\left|\Delta\varphi_{ij}\right| = \sqrt{\frac{\lambda_3}{(M-1)}\frac{\left(\lambda_i+\lambda_j-\lambda_3\right)}{\left(\lambda_i-\lambda_j\right)^2}}, i \neq j(i,j=1,2,3), \quad \text{(A1)}$$

where λ_1, λ_2 and λ_3 are maximum, intermediate and minimum eigenvalues, respectively, of the covariance matrix for COM method, and M is number of data points used in the analysis [*Khrabrov and Sonnerup*, 1998b; *Sonnerup and Scheible*, 1998, equation 8.23]. The above equation represents the rotation of eigenvector x_i toward or away from eigenvector x_j.

[47] The statistical uncertainty in a given vector **A** along the normal direction is given by

$$|\Delta\langle \mathbf{A}\cdot\mathbf{x_3}\rangle| = \sqrt{\frac{\lambda_3}{(M-1)} + \left(\Delta\varphi_{13}\mathbf{x_1}\cdot\langle\mathbf{A}\rangle\right)^2 + \left(\Delta\varphi_{23}\mathbf{x_2}\cdot\langle\mathbf{A}\rangle\right)^2} \tag{A2}$$

where $\mathbf{x_1}$, $\mathbf{x_2}$ and $\mathbf{x_3}$ are the eigenvectors corresponding to eigenvalues λ_1, λ_2 and λ_3, respectively [*Sonnerup and Scheible*, 1998, equation 8.24] and the angular brackets represent the average of the quantity enclosed. The above formula accounts only for the statistical uncertainties in the direction of the normal vector. Similar expressions are used to calculate the statistical uncertainty in the other two components. We have applied these expressions to averaged values of magnetic field, plasma velocity, magnetopause velocity and the current density from curlometer and single-spacecraft method to obtain the statistical uncertainty in all quantities.

[48] When calculating the energy conversion (equation (1)), the uncertainties in different variables, computed using equation (A2), must be propagated to obtain the uncertainty in the energy conversion estimated. In this study we estimate the uncertainty using the variance propagation method [*Bevington*, 1969; *Bevington and Robinson*, 2003]. For a function $x = f(u, v, ..)$, the variance of x, can be expressed in terms of variances of u and v using

$$\sigma_x^2 = \sigma_u^2\left(\frac{\partial x}{\partial u}\right)^2 + \sigma_v^2\left(\frac{\partial x}{\partial v}\right)^2 + 2\sigma_{uv}^2\frac{\partial x}{\partial u}\frac{\partial x}{\partial v} + .. \tag{A3}$$

where σ_x^2, σ_u^2 and σ_v^2 are variances of x, u and v, respectively and σ_{uv}^2 is the covariance between variables u and v. The higher order terms and the covariance term in equation (A3) can be neglected as they either vanish or their contribution is very small and are not used in the error propagation.

[49] Let us write $\mathbf{K} = \mathbf{J}\times\mathbf{B}$ and the three components are given by

$$\begin{pmatrix} K_l \\ K_m \\ K_n \end{pmatrix} = \begin{pmatrix} J_mB_n - J_nB_m \\ J_nB_l - J_lB_n \\ J_lB_m - J_mB_l \end{pmatrix} \tag{A4}$$

where we used **l**, **m**, and **n** instead of $\mathbf{x_1}$, $\mathbf{x_2}$, and $\mathbf{x_3}$, respectively. The statistical uncertainties in **J** and **B** estimated using equation (A2) should be propagated according to equation (A3) to obtain uncertainties in **K**. The uncertainty in each component of **K** is obtained by adding the uncertainties from the two terms on the right hand side of equation (A4). For example, the uncertainty for K_l is obtained by adding the uncertainties from J_mB_n and J_nB_m. These uncertainties are calculated following equation (A3). For K_l, the uncertainty is given by

$$\Delta K_l^2 = \Delta J_m^2B_n^2 + \Delta B_n^2J_m^2 + \Delta J_n^2B_m^2 + \Delta B_m^2J_n^2 \tag{A5}$$

where we have replaced the variances given in equation (A3) with the statistical uncertainties for the respective variables, i.e ΔJ_i^2 and ΔB_i^2. Similarly, we obtain ΔK_m^2 and ΔK_n^2, the uncertainties in other directions.

[50] Now let us say $q = \mathbf{K}\cdot\mathbf{V}$ and the uncertainty in q is obtained by adding the uncertainties in K_lV_l, K_mV_m and K_nV_n. This is given by,

$$\Delta q^2 = \Delta K_l^2V_l^2 + \Delta V_l^2K_l^2 + \Delta K_m^2V_m^2 + \Delta V_m^2K_m^2 + \Delta K_n^2V_n^2 + \Delta V_n^2K_n^2 \tag{A6}$$

where ΔV_i ($i = l, m, n$) is the statistical uncertainty in the plasma velocity. So far we have calculated the uncertainty Δq in the vector triple product $q = \mathbf{J}\times\mathbf{B}\cdot\mathbf{V}$. Now, we follow equation (A3) to calculate the uncertainty in the integrand of equation (1), i.e. multiplication of q with $|V_{mp}|$.

[51] Now the Final uncertainty in equation (1) is given by

$$\Delta Q = \int \sqrt{\Delta q^2V_{mp}^2 + \Delta V_{mp}^2q^2}\ \ dt \quad \left(Wm^{-2}\right) \tag{A7}$$

where ΔV_{mp} is the uncertainty in magnetopause speed along the normal direction. The uncertainties deduced here contain the statistical uncertainties in the eigenvectors while systematic errors caused by deviations from planarity assumption are not included.

[52] **Acknowledgments.** The Cluster data have been retrieved from the Cluster Active Archive (CAA), and we thank Harri Laakso and team for maintaining the system. We also thank the FGM and CIS instrument teams for their efforts in operating the instruments. Part of the analysis is done with QSAS software provided by Imperial College London and Queen Mary, University of London. The research leading to these results has received funding from the European Research Council under the European Community's Seventh Framework Programme (FP7/2007-2013)/ERC Starting Grant agreement 200141-QuESpace. The work of MP is supported by the Academy of Finland.

[53] Masaki Fujimoto thanks the reviewers for their assistance in evaluating this paper.

References

Akasofu, S.-I. (1981), Energy coupling between the solar wind and the magnetosphere, *Space Sci. Rev.*, *28*, 121–190.

Axford, W. I., and C. O. Hines (1961), A unifying theory of high-latitude geophysical phenomena and geomagnetic storms, *Can. J. Phys.*, *39*, 1433–1464.

Balogh, A., et al. (2001), The Cluster magnetic field investigation: Overview of in-flight performance and initial results, *Ann. Geophys.*, *19*, 1207–1217.

Bevington, P. R. (1969), *Data Reduction and Error Analysis for the Physical Sciences*, McGraw-Hill, New York.

Bevington, P. R., and D. K. Robinson (2003), *Data Reduction and Error Analysis for the Physical Sciences*, McGraw-Hill, New York.

de Hoffmann, F., and E. Teller (1950), Magneto-hydrodynamic shocks, *Phys. Rev.*, *80*, 692–703.

Dungey, J. W. (1961), Interplanetary field and the auroral zones, *Phys. Rev. Lett.*, *6*, 47–48.

Dunlop, M. W., A. Balogh, K.-H. Glassmeier, and P. Robert (2002), Four-point Cluster application of magnetic field analysis tools: The Curlometer, *J. Geophys. Res.*, *107*(A11), 1384, doi:10.1029/2001JA005088.

Dunlop, M. W., et al. (2006), The curlometer and other multi-point analysis, in *Proceedings of the Cluster and Double Star Symposium: 5th Anniversary of Cluster in Space* [CD-ROM], *Eur. Space Agency Spec. Publ.*, *ESA SP-598*.

Escoubet, C. P., M. Fehringer, and M. Goldstein (2001), The Cluster mission, *Ann. Geophys.*, *19*, 1197–1200.

Haaland, S. E., et al. (2004), Four-spacecraft determination of magnetopause orientation, motion and thickness: Comparison with results from single-spacecraft methods, *Ann. Geophys.*, *22*, 1347–1365.

Haaland, S. E., B. U. Ö. Sonnerup, G. Paschmann, E. Georgescu, A. Balogh, B. Klecker, H. Réme, and A. Vaivads (2006), Discontinuity analysis with Cluster, in *Proceedings of the Cluster and Double Star Symposium: 5th Anniversary of Cluster in Space* [CD-ROM], *Eur. Space Agency Spec. Publ.*, *ESA SP-598*.

Khrabrov, A. V., and B. U. Ö. Sonnerup (1998a), Orientation and motion of current layers: Minimization of the Faraday residue, *Geophys. Res. Lett.*, *25*, 2373–2376.

Khrabrov, A. V., and B. U. Ö. Sonnerup (1998b), Error estimates for minimum variance analysis, *J. Geophys. Res.*, *103*, 6641–6651.

Laitinen, T. V., P. Janhunen, T. I. Pulkkinen, M. Palmroth, and H. E. J. Koskinen (2006), On the characterization of magnetic reconnection in global MHD simulations, *Ann. Geophys.*, *24*, 3059–3069.

Laitinen, T. V., M. Palmroth, T. I. Pulkkinen, P. Janhunen, and H. E. J. Koskinen (2007), Continuous reconnection line and pressure-dependent energy conversion on the magnetopause in a global MHD model, *J. Geophys. Res.*, *112*, A11201, doi:10.1029/2007JA012352.

Lundin, R., and D. S. Evans (1985), Boundary layer plasmas as a source for high-latitude, early afternoon, auroral arcs, *Planet. Space Sci.*, *33*, 1389–1406.

Palmroth, M., T. I. Pulkkinen, P. Janhunen, and C.-C. Wu (2003), Storm time energy transfer in global MHD simulation, *J. Geophys. Res.*, *108*(A1), 1048, doi:10.1029/2002JA009446.

Palmroth, M., T. V. Laitinen, and T. I. Pulkkinen (2006), Magnetopause energy and mass transfer: Results from a global MHD simulation, *Ann. Geophys.*, *24*, 3467–3480.

Palmroth, M., T. V. Laitinen, C. R. Anekallu, T. I. Pulkkinen, M. Dunlop, E. A. Lucek, and I. Dandouras (2011), Spatial dependence of magnetopause energy transfer: Cluster measurements verifying global simulations, *Ann. Geophys.*, *29*, 823–838.

Panov, E. V., J. Büchner, M. Fränz, A. Korth, S. P. Savin, H. Réme, and K.-H. Fornacon (2008), High-latitude Earth's magnetopause outside the cusp: Cluster observations, *J. Geophys. Res.*, *113*, A01220, doi:10.1029/2006JA012123.

Paschmann, G., S. Haaland, B. U. Ö. Sonnerup, H. Hasegawa, E. Georgescu, B. Klecker, T. D. Phan, H. Réme, and A. Vaivads (2005), Characteristics of the neartail dawn magnetopause and boundary layer, *Ann. Geophys.*, *23*, 1481–1497.

Réme, H., et al. (2001), First multispacecraft ion measurements in and near the Earth's magnetosphere with the identical Cluster ion spectrometry (CIS) experiment, *Ann. Geophys.*, *19*, 1303–1354.

Robert, P., M. W. Dunlop, A. Roux, and G. Chanteur (1998), Accuracy of current density determination, in *Analysis Methods for Multispacecraft Data*, *ISSI Sci. Rep.*, *SR-001*, pp. 395–418.

Rosenqvist, L., S. Buchert, H. Opgenoorth, A. Vaivads, and G. Lu (2006), Magnetospheric energy budget during huge geomagnetic activity using Cluster and ground-based data, *J. Geophys. Res.*, *111*, A10211, doi:10.1029/2006JA011608.

Rosenqvist, L., A. Vaivads, A. Retinó, T. Phan, H. J. Opgenoorth, I. Dandouras, and S. Buchert (2008a), Modulated reconnection rate and energy conversion at the magnetopause under steady IMF conditions, *Geophys. Res. Lett.*, *35*, L08104, doi:10.1029/2007GL032868.

Rosenqvist, L., H. J. Opgenoorth, L. Rastaetter, A. Vaivads, and I. Dandouras (2008b), Comparison of local energy conversion estimates from Cluster with global MHD simulations, *Geophys. Res. Lett.*, *35*, L21104, doi:10.1029/2008GL035854.

Russell, C. T., and R. C. Elphic (1978), Initial ISEE magnetometer results: Magnetopause observation, *Space Sci. Rev.*, *22*, 681–715.

Russell, C. T., and R. C. Elphic (1979), ISEE observations of flux transfer events at the dayside magnetopause, *Geophys. Res. Lett.*, *6*, 33–36.

Russell, C. T., M. M. Mellott, E. J. Smith, and J. H. King (1983), Multiple spacecraft observations of interplanetary shocks: Four spacecraft determination of shock normals, *J. Geophys. Res.*, *88*, 4739–4748.

Sonnerup, B. U. Ö., and M. Scheible (1998), Minimum and maximum variance analysis, in *Analysis Methods for Multi-Spacecraft Data*, edited by G. Paschmann and P. W. Daly, *Eur. Space Agency Spec. Publ.*, *ESA SP-SR-001*, pp. 185–220.

Sonnerup, B. U. Ö., S. Haaland, G. Paschmann, B. Lavraud, M. W. Dunlop, H. Réme, and A. Balogh (2004), Orientation and motion of a discontinuity from single-spacecraft measurements of plasma velocity and density: Minimum mass flux residue, *J. Geophys. Res.*, *109*, A03221, doi:10.1029/2003JA010230.

Sonnerup, B. U. Ö., S. Haaland, G. Paschmann, M. W. Dunlop, H. Réme, and A. Balogh (2006), Orientation and motion of a plasma discontinuity from single-spacecraft measurements: Generic residue analysis of Cluster data, *J. Geophys. Res.*, *111*, A05203, doi:10.1029/2005JA011538.

C. R. Anekallu and M. Palmroth, Finnish Meteorological Institute, Helsinki FI-00101, Finland. (chandrasekhar.anekallu@fmi.fi)

I. Dandouras, CESR, Université de Toulouse, Toulouse F-31028, France.

S. E. Haaland, Max-Planck-Institute for Solar System Research, Katlenburg-Lindau D-37191, Germany.

E. Lucek, Space and Atmospheric Physics, Imperial College, London SW7 2AZ, UK.

T. I. Pulkkinen, School of Electrical Engineering, Aalto University, Aalto FI-00101, Finland.